2-D TOMOGRAPHIC RECONSTRUCTUION OF INSTANT OH*-CHEMILUMINESCENCE DISTRIBUTIONS IN TURBULENT FLAMES

Nikolay B. Anikin*, Rainer Suntz*, Henning Bockhorn**
e-mail: anikin@ict.uni-karlsruhe.de
*Institute for Chemical Technology and Polymer Chemistry, Karlsruhe Institute of Technology; Kaiserstrasse 12, 76131 Karlsruhe, Germany
**Engler-Bunte Institute, Karlsruhe Institute of Technology, Kaiserstrasse 12, 76131 Karlsruhe, Germany

Abstract
A newly designed fast tomographic reconstruction device [1] has been applied to detect the 2-D chemiluminescence distributions of OH* in the reaction zones of turbulent flames. A series of single-shot experiments has been carried out in two non-premixed turbulent flames at flow velocities 0.43 m/s and 4 m/s and flame diameters up to 60 mm, respectively. The emission of OH* originating from the flame front has been registered with a spatial resolution of ~1 mm and an exposure time down to 200 µs. Further, 2-D distributions of OH*-emission were reconstructed from the experimental data using a numerical procedure solving the inverse problem of tomography [1, and references therein].

Introduction
The heat release rate is the dominating physical quantity, which considerably determines the stability of combustion processes [2]. Unfortunately, this quantity is experimentally not accessible by implication. However, there are some indicators which give useful information about the heat release rate. The most convincing one is the concentration of the formyl-radical [3,4], which can be detected by laser-induced fluorescence (LIF). Because the latter is accompanied with very essential experimental efforts, similar information [4] can be obtained simply by simultaneous OH- and CH_2O-LIF-measurements.

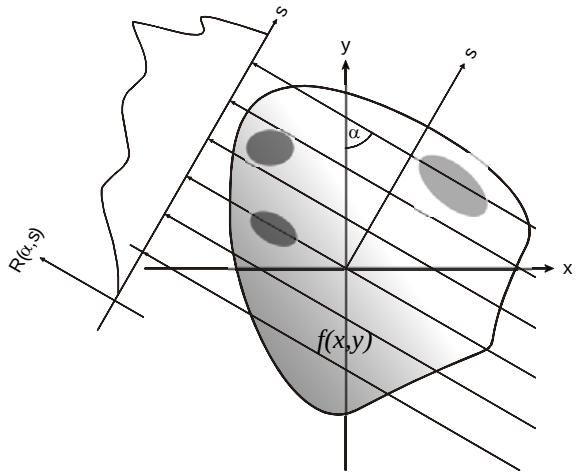

Figure 1. Schematic illustration of two-dimensional Radon transform.

Another approach to achieve information about the heat release rate is based on the detection of chemiluminescence signals originating from flame intermediates, especially OH* [5]. For axis-symmetric flames spatially resolved OH*-measurements can easily be obtained by Abel-inversion- or onion-peeling-methods using a single (fixed) intensified CCD-camera

(ICCD) [6]. However, if instantaneous, spatially resolved OH*-distributions from turbulent flames are investigated, computerised tomography methods have to be applied.

Essentially asymmetrical flames can only be investigated using detectors of a special design. The reconstruction of the chemiluminescence distribution is achieved solving the inverse problem of tomography based upon Radon integral transform.

The Radon integral transform $R(\alpha,s)$ [7] is given by

$$R(\alpha, s) = \iint \delta[(x\cos\alpha + y\sin\alpha) - s] f(x, y)\, dxdy, \quad (1)$$

with $\delta[(x\cos\alpha + y\sin\alpha) - s]$ the one-dimensional Dirac delta function. As illustrated in Figure 1, the OH*-chemiluminescence emission intensity $f(x,y)$ only contributes to the integrated signal $R(\alpha,s)$ along the path of the ray $s = x\cos\alpha + y\sin\alpha$.

For practical applications of tomography the Radon transform $R(\alpha,s)$ has to be measured experimentally across the total projected size of the object under investigation (e.g. flame) for various projection angles α_κ, ranging from 0° to 180°. The graphical representations of $R(\alpha_\kappa,s)$ are also called *sinograms* (see e.g. Figure 7). For steady state cases, $R(\alpha_\kappa,s)$ is measured at different angles α_κ by a single linear (one-dimensional) detector, which is rotated around the object under investigation. However, for e.g. (unsteady) turbulent flames this strategy fails, because temporal fluctuations of $f(x,y)$ are fast compared to the time necessary to rotate the detector around the object under investigation. Consequently, a preselected number of detectors (k = 1,...,N) has to be positioned at all detection angles α_κ in order to detect $R(\alpha_\kappa,s)$ simultaneously.

In this paper we present a tomographic device, which satisfies the prerequisites mentioned above. Therefore, the apparatus can be used for time resolved tomography applications, e.g. turbulent flames.

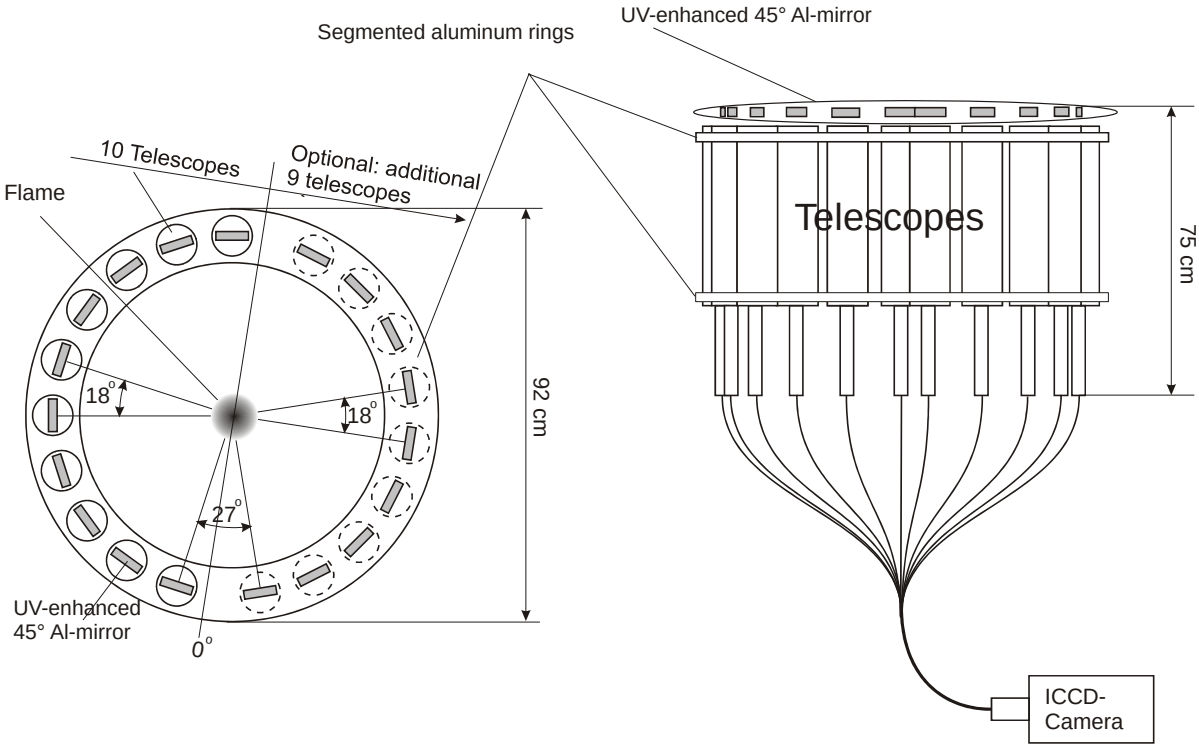

Figure 2. Schematic illustration of the tomographic reconstruction setup. Left figure: top view, right figure: side view.

Tomographic setup

The tomographic system is extensively described in [1]. Ten angular equally separated Kepler-telescopes surrounding the flame in a semi-circle. These telescopes serve for two major purposes: 1) to provide selective transmission of well defined (parallel and coplanar) rays, which is a prerequisite for the tomographic reconstruction of *f(x,y)*. 2) To adopt the image size of the flame to the detector size.

As shown in Figure 2, the telescopes are arranged vertically in order to minimize the horizontal dimensions of the device. The OH*-emission (λ_{cw}= 307 nm) originating from the flame is deflected in the vertical direction by UV-enhanced 45°-mirrors mounted on top of each telescope.

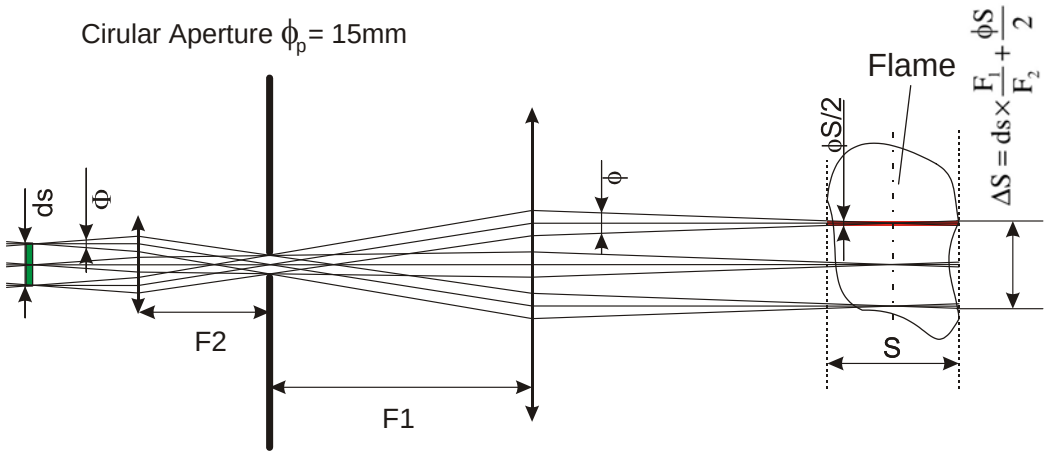

Figure 3. Schematic illustration of the optical resolution of the telescopes (45° deflection mirror is omitted).

The telescopes consist of two anti-reflection coated fused silica lenses, respectively: the objective lens (focal length F_1= 474 ± 2.3 mm (at 310 nm); diameter ϕ_1 = 75 mm) and the ocular lens (focal length F_2= 71 ± 0.5 mm (at 310 nm); diameter ϕ_2= 30 mm).

A circular aperture placed in the focal plane of the telescope restricts the transmission of divergent rays emitted by the flame. The divergence of transmitted rays and therefore the resolution of the device (see Figure 3) are controlled by the size of this aperture ϕ_p. In our arrangement ϕ_p= 15 mm is chosen because it turns out that this value represents a good compromise between the signal strength on the one hand and the optical resolution of the system (~1mm) on the other hand.

Each telescope projects the image of the flame onto a face of an optical cable consisting of 90 single fibres (core diameter: 100 μm), respectively. These fibres are arranged in a single row side by side (center to center separation: 125 μm) forming a linear array. The magnification factor of the telescope is F_1/F_2= 6.7 at 310 nm. The maximal size of the object under investigation is approximately 70 mm and mainly restricted by the clear aperture of the first lens.

The linear arrays of fibres transmit solely OH*-chemiluminescence signals originating from flat narrow layers of the flame. The opposite ends of these cables are merged together to a rectangular arrangement of 10 rows consisting of 90 fibres each. This arrangement is connected to an intensified CCD-camera (Princeton Instruments, ICCD PIMAX 512 RB) with a 1:1-optical relay system. The latter consists of a pair of anti-reflection coated fused silica aspheric lenses (F = 120 mm (at 310 nm), ϕ = 50 mm, respectively). Thus, the setup registers simultaneously linear images of flame planes obtained from parallel rays at 10 different

angles, respectively. All detection planes of the device were aligned with very good accuracy (< 0.4 mm) with respect to each other. The adjustment procedure is described in [1].

The registered image of the ICCD-camera is converted into a (α x s)-matrix by a special computer programme. The angle (α)- and the number of fibre (s)- dependant elements of the matrix represent the integral intensity over the image area of each particular (α, s) fibre, respectively. Therefore, the signal strength-information of the matrix elements (α, s) is the Radon transform $R(\alpha,s)$ multiplied with some sensitivity function $F_s(a,s)$, which is individual for each particular fibre.

The device was calibrated using a laminar premixed flat flame of rectangular shape (5 mm x 70 mm). The latter was placed in the centre of the setup with respect to the vertical and horizontal position, respectively. Each detection channel (α,s), consisting of (1) mirror, (2) telescope, (3) the individual fibre (α,s) and (4) the corresponding area of the ICCD was calibrated as a solid unit. Having assumed the uniformity of the flat flame, the sensitivity function $F_s(a,s)$ of each particular channel (α, s) was obtained by measuring the OH*-signal intensity of the flat flame orientated parallel to the face of the corresponding telescope.

Tomographic reconstruction procedure

Equation (1) is a Fredholm integral equation of first kind with respect to the unknown function $f(x,y)$. Therefore, the reconstruction of $f(x,y)$ from the measured Radon transform $R(\alpha,s)$ (so called inverse problem of tomography) is a mathematically ill-posed problem, which can only be solved approximately [8].

In a first step we discretize $f(x,y)$ and $R(\alpha,s)$ according to our detection scheme (10 angles, 90 fibres). The step size of the discretization is chosen according to the separation between two adjacent fibres multiplied by the demagnification factor of the telescope (0.83 mm) and the angle separation of the telescopes (18°). The discrete Radon transform is given by

$$R_{k,n} = \sum_{i=1,\, j=1}^{i=I,\, j=J} f_{i,j} \cdot D_{k,n}^{i,j} \,, \tag{2}$$

with $f_{i,j}$ the emission intensity for the numerical cell (i,j). I x J= 90 x 90 = 8100 is the total number of numerical grid points. $R_{k,n}$ is the Radon-transformed intensity (projection) for ray-number k at angle n *(k-n ray)* with K= 90 the number of rays and N= 10 the number of angles. $D_{k,n}^{i,j}$ represents the projection matrix.

For reasons shown in [1], the minimization of the regularized function $\Phi(\boldsymbol{f},\lambda)$ is the method of choice for our purposes in order to reconstruct the OH*-distribution. In a discrete form this function is given by

$$\Phi(f_{i,j},\lambda) = \sum_{k=1,n=1}^{k=K,n=N} \left(R_{k,n} - \sum_{i=1,\, j=1}^{i=I,\, j=J} f_{i,j} \cdot D_{k,n}^{i,j} \right)^2 + \lambda \sum_{i=1,\, j=1}^{i=I,\, j=J} \left(f_{i,j} \right)^2, \tag{3}$$

with the regularisation parameter λ. This parameter serves as a weighting factor of the last term on the right hand side of the formula. The latter serves as a filter, which smoothes the solution of $f(x,y)$. The function $\Phi(f_{i,j},\lambda)$ is minimized by an iterative variation of the $f_{i,j}$-distribution based on the steepest descent method. The detailed description of both, the proper choice of the value of λ and the mathematical procedure in general, are given in [1].

Burner of turbulent flame

In order to investigate the behaviour of our apparatus, first we tested the tomographic device by reconstructing laminar premixed flat flames of different shapes as well as laminar diffusion flames [1]. Even for signal exposure times down to 100 μs these investigations preceded successfully. Therefore, in this paper we investigate OH*-chemiluminescence distribution from turbulent flames.

These investigations were carried out using a burner similar to the one described in reference [9]. In Figure 4 a sketch of the burner is given. In contradistinctions to [9], our burner has the perforated plate and a shortened plenum. The porosity of the plate is 0.2 and the diameter of the perforations is 1 mm. The fuel supply tube positioned at the axis of the burner has six radial openings 2 mm below of the bluff-body edge. The openings serve for the CH_4-supply of the annular nozzle (0.7 mm in height showed in the Figure 4) of the bluff-body.

For the investigations two different non-premixed methane-air flames are used:

1) The first one was a flame slightly (~5mm) lifted above the bluff-body. In the following this flames is called *cylindrical* flame, since the cross-section of the flame changed downstream slightly. The throughputs were 10 sl/min for air and 2 sl/min for CH_4. Measurements were carried out at 13.2 and 27.4 mm height above the bluff-body edge, respectively.
2) The second flame was attached to the bluff-body. Since the flame expands downstream with the nearly conical shape it is called *conical* flame. The throughputs were 100 sl/min for air and 2 sl/min for CH_4. Measurements were carried out at 2.0, 7.6, 13.2, 18.8 and 24.4 mm height above the bluff-body edge, respectively.

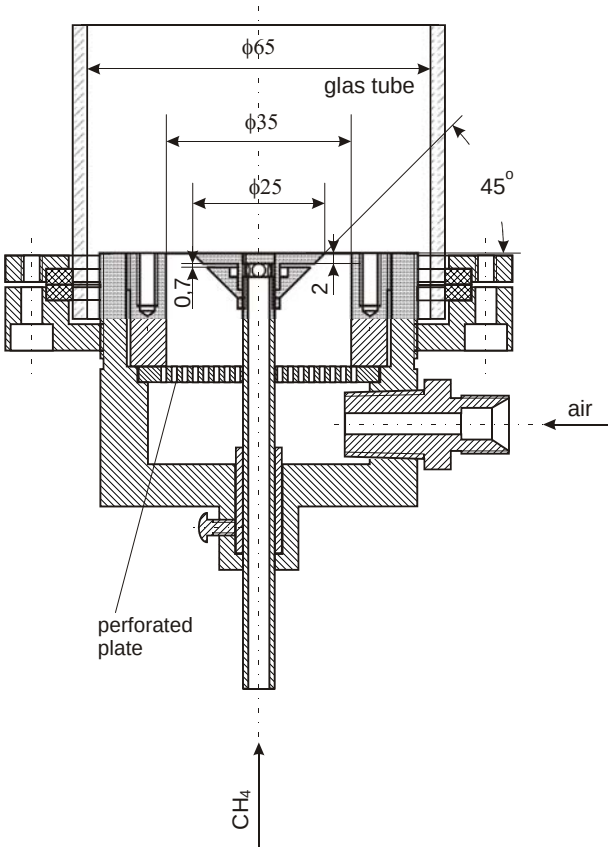

Figure 4. Axial cross-section of the turbulent burner.

Results and discussion

The 2-D distributions of OH*-chemiluminescence in these two flames were reconstructed from the experimentally obtained Radon transforms by means of the iterative procedure mentioned above.

The reconstructed distributions of the OH*-emission of the *cylindrical* flame are represented in the Figure 5. For this flame the exit velocity of the flow (0.43 m/s) is actually equal to the maximal value of the laminar burning velocity (0.42 m/s, see e.g. [10]) for

methane-air mixtures. Therefore, the flame is nearly laminar and behaves similar to a usual laminar diffusion flame. For this reason it is interesting to compare the recent results with those obtained in laminar diffusion flames and reported in [1].

In both cases the shapes of the cross-sections of both flames are similar to a thin continuous ring. Thicknesses of both flames (2 points of the numerical grid or 1.7mm for the diffusion flame in [1] and 2-3 points of the grid or 1.7-2.5 mm for the *cylindrical* flame) were close to the resolution limit (two point of the numerical grid or 1.7mm) of the reconstruction.

The flame from [1] has circular shape and is stable in time. To the contrary, at the bottom cross-section (13.3mm) the *cylindrical* flame has almost regular hexagon shape (Figures 5 a), b) and c)).This is caused by the 6 radial openings in the fuel supply tube. Further downstream the shape is distorted essentially (compare Figures a), b) and c) with d), e) and f)).

From Figure 5 we see that the flame front pulsates (compare sizes of distributions in Figures 5 a) and d) with those of b) and e), respectively) keeping nearly permanent shape. In the upper cross-section, the amplitude of the pulsations is bigger, since the averaged flame front is essentially wide (~4mm for the upper cross-section and ~2.5mm for the bottom one) in this case (compare Figures 5 c) and f)).

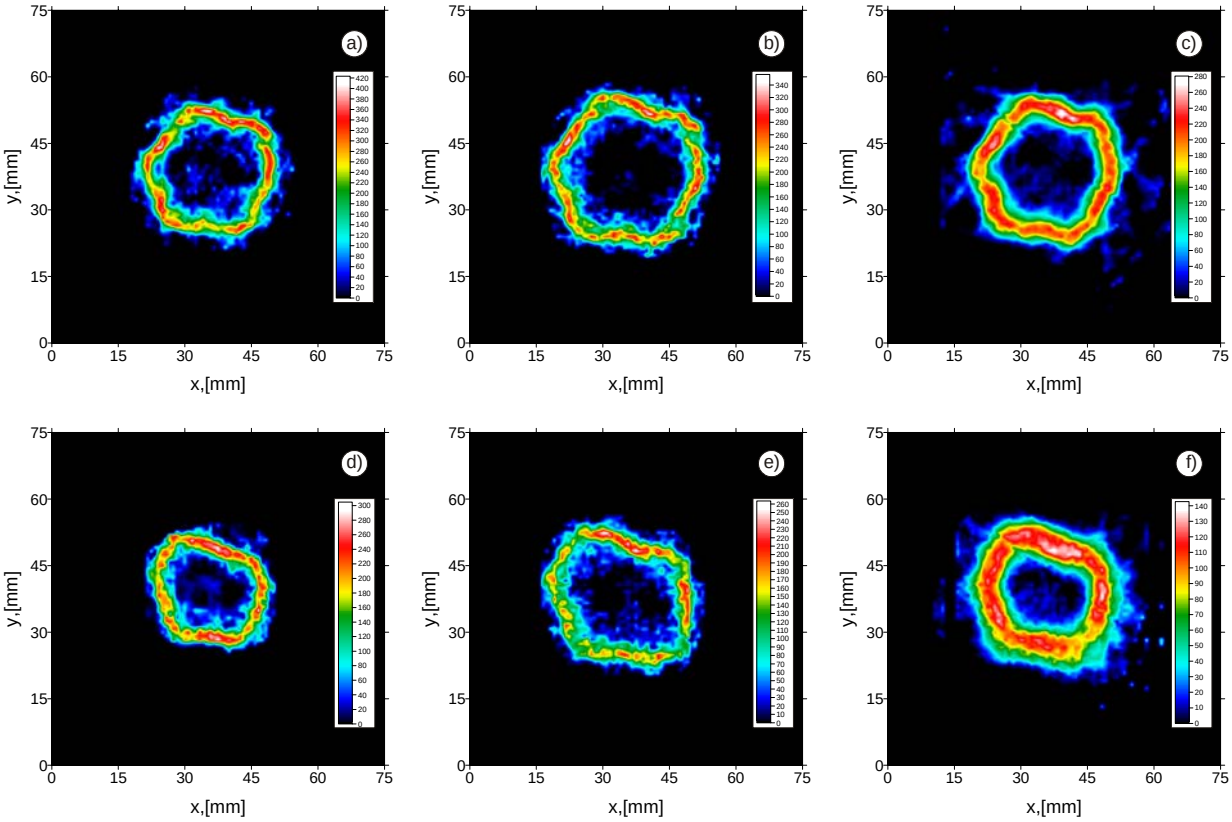

Figure 5. The reconstructed distributions of the OH*-emission of the nearly laminar (cylindrical) flame are represented in the horizontal planes at two heights above the bluff-body edge: Figures a), b) and c): 13.3 mm, d), e) and f): 27.2 mm. Figures c) and f) represent the reconstruction averaged over 20 single-shot measurements. Figures a), b), d), e) represent single-shot measurements. The exposure time was 1ms.

Thus, the apparatus allows reconstructing of 2-D maps of OH* in relatively complex flame – the specific configuration of the burner (the perforated grid and the bluff-body) provides the essential complexity of the flow. On the other hand, the flame front propagates slowly and the turbulence in it is actually weak.

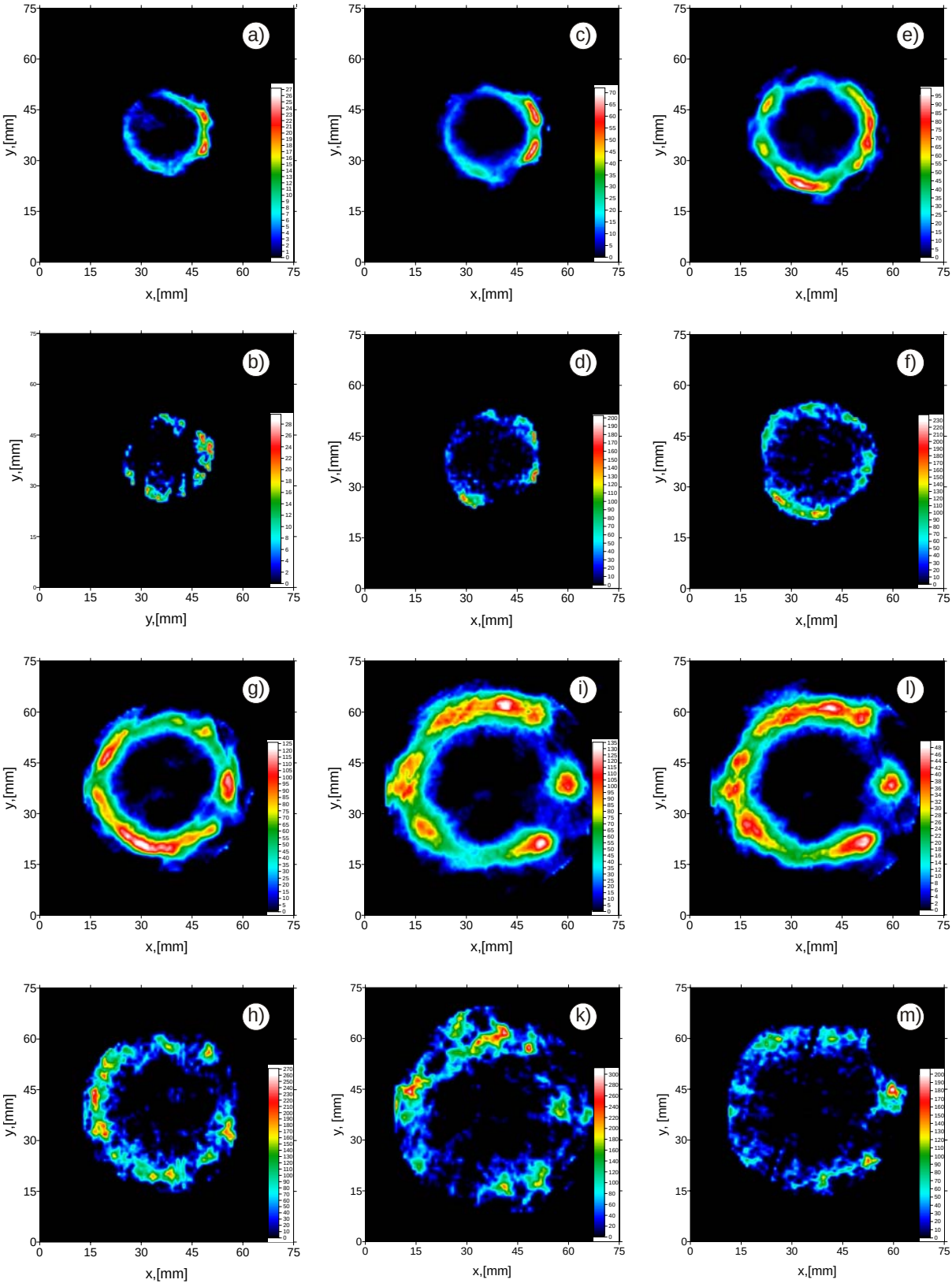

Figure 6. The reconstructed distributions of the OH*-emission of the turbulent (conical) flame are represented in the horizontal planes at various heights above the bluff-body edge: Figures a) and b): 2 mm, c) and d): 7.6 mm, e) and f): 13.3 mm, g) and h): 18.8 mm, and i), k), l) and m): 24.4 mm. Figures a), c), e), g), i), l) represent the reconstruction averaged over 60 single-shot measurements. Figures b), d), f), h), k), m) represent single-shot measurements. The exposure time for all Figures except l) and m) is 500 μs, for figures l) and m) it is 200 μs.

The next step of our investigation is the reconstruction of OH* distribution in the *conical* flame, which is strongly turbulent, because the exit velocity of the gas flow (~4m/s) is approximately one order of magnitude higher than the maximal value of the laminar burning velocity.

The reconstructed distributions of the OH*-emission of the *conical* flame at different heights above the bluff-body edge are represented in the Figure 6. Figures 6a), 6c), 6e), 6g), 6i), 6l) represent distributions reconstructed from the Radon transform obtained by averaging 60 single-shot events. The other figures are reconstructed distributions from single-shot measurements.

From the figure it becomes obvious that the *conical* flame consists of several leafs. This is a consequence of the six radial openings in the fuel supply tube. Dependant on the detection height, adjacent leafs of the flame more or less overlap with each other in the single-shot cases. In the averaged reconstructions, these leafs form a ring-like structure with some interruptions. At 2 mm height above the bluff-body (Figures 6a) and 6b)), the size of the flame is similar to the bluff-body diameter (25 mm). With increasing height the diameter of the flame increases more or less linearly reaching approximately 55 – 58 mm at 24.4 mm (Figures 6 i), 6k), 6l), 6m)). Simultaneously, the characteristic thickness of the flame zone rises from 2 – 3 mm at the lower height up to ~ 8 mm at the higher height above the burner. Both, the average as well as the single shot distributions show a similar shape and values for the OH*-chemiluminescence intensities. This indicates that the flame zone is actually thick otherwise the single shot measurements should give an essentially thinner flame width.

In contradiction to the average distributions, in the single shot reconstructions essential contributions of short wave structures are observed. The number of these contributions is noticeably increased if the exposure time is decreased (compare figures 6k) and 6m)). However, the average distributions are very similar in both cases (Figures 6i) and 6l)). This behavior could be explained by two different reasons:

1) Noise of the reconstruction is responsible for this behavior. The high frequency structures are caused by insufficient signal to noise ratio (SNR) of the single shot data. The SNR is improved with increasing exposure times for single shot measurements or by averaging single shot data over many events.
2) The proper short wave structure of the turbulent flame.

In order to find the right explanation we analyzed the sinograms of the flame at 24.4 mm height above the bluff-body edge. Figure 7 a), b), d) and e) depicts the sinograms for single shot measurements, whereas in Figure 7 c) the average of 60 single-shot measurements is given. Figures 7a), 7c) represent measured sinograms for the exposure time 500 μs in contrast to 200 μs for 7d). The OH*-distributions reconstructed from the sinograms 7a), 7c) and 7d) are depicted in figures 6k), 6i) and 6m), respectively. Figures 7b) and 7e) represent sinograms, which are (re)calculated from the distributions 6k) and 6m) using formula (2), respectively. From the comparison of the average sinogram (Figures 7c) with the single shot ones (Figures 7a) and 7d)) it becomes obvious, that the latter have an essential number of short wave structures. Additionally, they are markedly increased for the shorter exposure time (compare Figures 7a) and 7d)).

The comparison between the measured (Figure 7 a) and d)) and the corresponding (re)calculated (Figures 7 b) and e)) sinograms shows that the short wave contributions in the (re)calculated sinograms confidently reflects the contributions in the respective measured ones. This is an indication that the short wave structures reflect an inner fine structure of the turbulent flame rather than being an artifact caused by noise. Therefore, an instant emission distribution of a flame can be reconstructed within the spatial resolution of the device (~ 1 mm, see [1]).

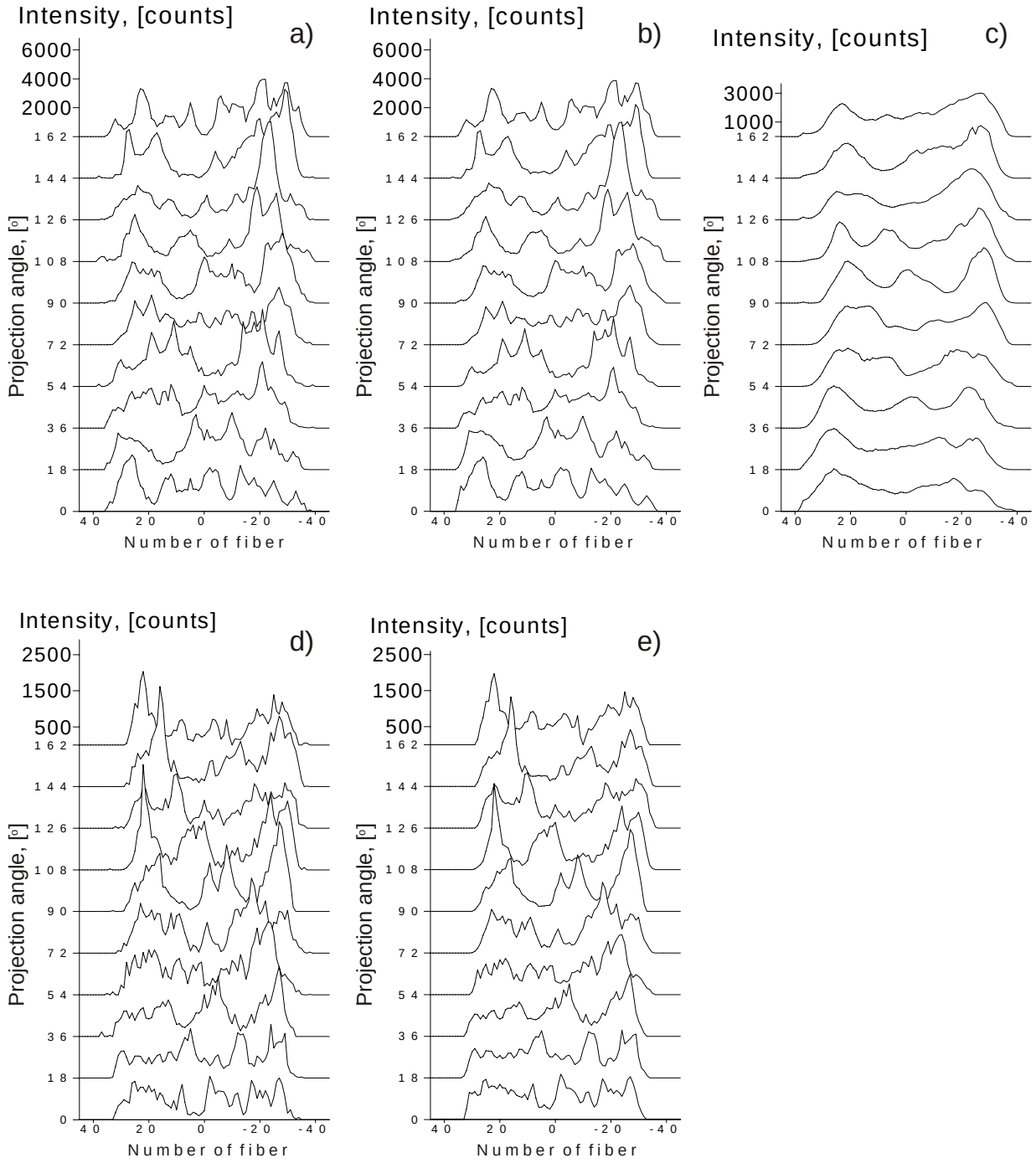

Figure 7. Sinograms at 24.4 mm height above the bluff-body edge. a), c) and d) are measured, b) and e) are calculated sinograms (explanation see text). a), b), d), e) represent results from single-shot events and c) is obtained by averaging 60 single-shot measurements. Exposure times are: 500 μs for a), b) and c); 200 μs for d) and e).

Conclusions

The fast tomographic device described in [1] has been applied to reconstruct the two-dimensional distributions of OH*-chemiluminescence in two non-premixed flames, one of which is essentially turbulent. For exposure times 200 and 500 μs, the 2-D-maps of OH* at the strongly turbulent flame have been achieved in 5 different cross-sections taken at different heights above the burner. The distribution analysis showed that the apparatus reconstruct the

fine structure of turbulent flames adequately, and can be used for instant spatially resolved measurements of OH*-emission in flames.

Acknowledgements
The authors gratefully acknowledge Deutsche Forschungsgemeinschaft DFG (Paket-Forschungsantrag: „Chemilumineszenz und Wärmefreisetzung“) for its financial support.

References

[1] Anikin N., Suntz R., Bockhorn H., “Tomographic reconstruction of the OH^*-chemiluminescence distribution in premixed and diffusion flames”, *Appl. Phys. B* 100: 675-694 (2010)
[2] Candel S., “Combustion Dynamics and Control: Progress and Challenges.”, *Proc. Combust. Inst.* 29: 1-28 (2002)
[3] Paul P.H. and Najm H.N., “Planar Laser-Induced Fluorescence Imaging of Flame Heat Release”, *Proc. Combust. Inst.* 27: 43-50 (1998)
[4] Rehm J.E. and Paul P.H., “Reaction Rate Imaging”, *Proc. Combust. Inst.* 28: 1775-1782 (2000)
[5] Dandy D.S. and Vosen S.R., Numerical and Experimental Studies of Hydroxyl Radical Chemiluminescence in Methane-Air Flames *Combust. Sci. and Tech.* 82:130-151 (1992)
[6] Hentschel J., Suntz R. and Bockhorn H., “Soot formation and oxidation in oscillating methane–air diffusion flames at elevated pressure”, *Applied Optics* 44: 6673-6681 (2005)
[7] Radon J., “Über die Bestimmung von Funktionen durch ihre Integralwerte längs gewisser Mannigfaltigkeiten”, *Ber. Verh. Sächs. Akad. Wiss. Leipzig, Math.-Nat. kl.* 69: 262-277 (1917)
[8] Tikhonov A.N. and Arsenin V.A., *Solution of Ill-posed Problems*, Winston & Sons, Washington, 1977, p. 258.
[9] Balachandran R., Ayoola B.O., Kaminski C.F., Dowling A.P., Mastorakos E., “Experimental investigation of the nonlinear response of turbulent premixed flames to imposed inlet velocity oscillations” *Combustion and Flame* 143: 37-55 (2005)
[10] Agrawal, D.D., “Experimental Determination of Burning Velocity of Methane-Air Mixtures in a Constant Volume Vessel”, *Combustion and Flame*, 42: 243-252 (1981)